ISSN 0915-633X

NATIONAL INSTITUTE FOR FUSION SCIENCE

Optimization of M=2 Stellarator

N. Nakajima, M. Yokoyama, M. Okamoto and J. Nührenberg

(Received - Nov. 28, 1996)

NIFS-470 Dec. 1996

RESEARCH REPORT
NIFS Series

NAGOYA, JAPAN

Optimization of M=2 Stellarator

Noriyoshi Nakajima, Masayuki Yokoyama, Masao Okamoto

National Institute for Fusion Science, 464-01, Japan

Jürgen Nührenberg

Max-Planck Institut für Plasmaphysik, EURATOM Association, Koitenhäger Landstrasse, D-17491 Greifswald, Germany

Abstract

Quasi-axisymmetric stellarator (QAS) configurations are considered for improvement of high energy reflected particle confinement. A reference QAS configuration with the field period of $M = 2$ has been obtained by the optimization of the shape of the confinement region. A wide operational regime, collisional (without net plasma current) and collisionless (with bootstrap current) equilibria, have been examined. The magnetic axis shift is rather large in collisional equilibrium in the reference QAS configuration. On the other hand, in collisionless equilibrium, the bootstrap current is evaluated self-consistently and its crucial role on reduction of magnetic axis shift is shown. The effects of important boundary harmonics on the magnetic configuration are considered, in particular, plasma boundary control has been investigated for reducing the Pfirsch-Schlüter current. Based on the plasma boundary control, we have obtained two QAS(-like) configurations with reduced magnetic axis shift. The basic properties for these two configurations are also explained.

Key Words: Stellarator optimization, Quasi-axisymmetric stellarator (QAS), Shape of the confinement region, Pfirsch-Schlüter current, Bootstrap current, Boozer coordinates, Magnetic spectra, Vertical elongation, Helical modulation, Triangularity.

1 Introduction

In order to optimize stellarators a difficult subject is the compatibility between high limit of MHD beta and good confinement of reflected high energy particles or alpha particles in a reactor. For obtaining the good confinement of reflected particles, several ways have been already proposed. One is the inner shift of the magnetic axis in heliotrons [1] such as Large Helical Device (LHD) [2]. The magnetic configuration with the magnetic axis of 15 cm shifted inward from the geometrical major radius of the device has been chosen as the standard configuration in LHD. There is no collisionless reflected particle loss from $r/a \lesssim 0.3$ at zero beta in the standard configuration. Here r/a denotes the normalized average plasma radius. On the other hand, in the W7-X [3], the dominant contribution of the plasma is the diamagnetic effect due to the reduction of finite beta induced currents such as Pfirsch-Schlüter and bootstrap currents for keeping the good quality of vacuum magnetic surfaces even in finite beta plasmas. The diamagnetic effect improves the reflected particle orbit in finite beta plasmas [4]. Quasi-helically symmetric (QHS) configurations [5] are another way to improve reflected particle confinement. In QHS stellarator, the essential point for improvement of reflected particle confinement is to eliminate toroidal effects and to restore helical symmetry for the magnetic field strength in magnetic coordinates. The HSX [6] is an example of this concept.

The magnetic configuration can be controlled by the plasma boundary control because MHD equilibria can be specified by boundary value problem with given pressure and current profiles [7]. Therefore, the magnetic configuration can be optimized to have desired physical criteria based on the plasma boundary control [8]. The QHS configuration and the W7-X configuration have been obtained by these procedures. The different desired physical criteria have led to the two different magnetic configurations. The quasi-axisymmetric stellarator (QAS) configuration is based on having the axisymmetric property for the magnetic field strength [9]. The external coil geometry, on the other hand, can be obtained by solving the magnetic field in the vacuum region as done by P.Merkel [10].

Neoclassical transport theory predicts that the bootstrap current can flow in stellarators as well as in tokamaks. The existence of the bootstrap current has been experimentally demonstrated both in tokamaks [11] and in stellarators [12] and it is reported that the bootstrap current is well described by the neoclassical transport theory [13]. Moreover, the bootstrap current has been recognized to play an important role in so called "reversed shear" mode in "advanced" tokamak operations [14]. Since the bootstrap current flows along the magnetic field lines, it has an important role as a net plasma current for MHD equilibrium and stability. Therefore, it is crucial to consider stellarator configuration optimization including the consistently evaluated bootstrap current.

This paper is organized as follows. In Section 2, a reference QAS configuration is briefly mentioned to clarify the basic properties. The effect of bootstrap current on MHD equilibrium is also examined. Section 3 will be devoted to show clearly the effects of the plasma boundary control on the magnetic configuration. The reduction of the magnetic axis shift for obtaining higher equilibrium beta limit, $\langle\beta\rangle_{eq}$, will be emphasized. The two QAS(-like) configurations with reduced magnetic axis shift are explained in Section 4. Finally, summary and some future works will be mentioned in Section 5.

2 Reference QAS configuration

Figure 1 shows the magnetic surface cross section of $M = 2$ QAS configuration at three different poloidal cross sections: $\phi = 0$, $\phi = (1/4)(2\pi/M)$ and $\phi = (1/2)(2\pi/M)$ with M the number of the field period and ϕ the geometrical toroidal angle. The plasma aspect ratio, A_p, is about 4.2 and it has a vacuum magnetic well of 0.6%. The magnetic well is defined by $(V'(0) - V'(\psi_T))/V'(0)$, where V is the volume enclosed by the magnetic surface corresponding to the toroidal flux ψ_T and the prime denotes the derivative with respect to ψ_T.

We have used the fixed boundary version of the VMEC [15] to calculate the finite beta MHD equilibria. The pressure profile is assumed as

$$P = P_0(1 - \psi_T)^2 . \tag{1}$$

It is noted that this pressure profile is frequently observed in CHS experiments [16].

We will consider a wide operational regime such as (1) collisional plasma without the net plasma current corresponding to high density, low temperature plasmas, and (2) collisionless plasma with bootstrap current corresponding to low density, high temperature plasmas. In collisionless plasmas, it is crucial to evaluate the bootstrap current self-consistently and examine its effect on the MHD equilibrium and stability. In the present study, we calculated the bootstrap current by following Watanabe et al. [17], where the connection formula was developed to evaluate the bootstrap current in the whole range of collisionality.

The major radius of the device, R, is assumed to be 2 m and the average magnetic field strength on the magnetic axis is to be 2 T in the following calculations.

Figure 2.1 shows magnetic surface cross sections of the reference QAS configuration at (a) $\langle\beta\rangle = 1.15\%$ for collisional equilibrium and (b) $\langle\beta\rangle = 1.18\%$ for collisionless equilibrium. The rotational transform ι and magnetic well depth (%) for both equilibria are shown in Fig/ 2.2 (a) and (b), respectively. The rotational transform and magnetic well depth for zero beta are also shown for reference. When we define the magnetic axis shift by Δ/a, where Δ denotes the difference of the average position of the magnetic axis in major radius direction, R_{00}, from its value at zero beta, $\Delta/a \sim 37\%$ for collisional equilibrium at $\langle\beta\rangle = 1.15\%$. This large magnetic axis shift implies a low $\langle\beta\rangle_{eq}$; the magnetic well is significantly enhanced as shown in Fig. 2.2(a) due to the large axis shift.

The investigation of MHD stability has been restricted only to ideal Mercier mode [18] to have a first insight. This collisional equilibrium is stable against the ideal Mercier mode at least up to this beta value. For the calculations of bootstrap current, we have assumed that the plasma is composed of only electrons and protons and they have the same temperature and density with the profile as

$$n_e(\psi_T) = n_i(\psi_T) = 10^{20}(1-\psi_T)\,\mathrm{m}^{-3}, \quad T_e(\psi_T) = T_i(\psi_T) = 1.5(1-\psi_T)\,\mathrm{keV}, \tag{2}$$

where the subscripts e and i denote electron and ion, respectrively. It is noted that the contribution of the radial electric field to the bootstrap current [19] vanishes because electrons and ions have the same collisionality for the assumed density and temperature profiles. The calculated total bootstrap current is about 150 kA for collisionless equilibrium, which increases the rotational transform except for the region near the magnetic axis. The magnetic axis shift is relatively suppressed ($\Delta/a \sim 17\%$) compared to the collisional equilibrium. This fact implies the improvement of $\langle\beta\rangle_{eq}$ with bootstrap current. The magnetic well enhancement is not so large as shown in Fig. 2.2(b) due to the smaller magnetic axis shift; however, this magnetic well is sufficient to keep the ideal Mercier modes stable at least up to this beta value. It is noted that the ι profile is the same as the safety factor q profile with the reversed shear in tokamak operation with the large fraction of the bootstrap current [14].

Figure 3 shows the magnetic field spectra in Boozer coordinates [20] for (a) zero beta and (b) $\langle\beta\rangle = 1.15\%$ for the collisional equilibrium shown in Fig. 2.1. The magnetic field strength B is expressed as

$$B = \sum_{mn} B_{mn}(r)\cos(m\theta_B - nM\zeta_B), \tag{3}$$

where θ_B (ζ_B) is the poloidal (toroidal) angle in the Boozer coordinates and r denotes the average radius with m (n) the poloidal (toroidal) mode number. Here it is noted that the toroidal mode number is devided by $M = 2$. The B_{00} curve denotes the difference of B_{00} between at r and at the magnetic axis, $B_{00}(r) - B_{00}(0)$. All other components are normalized with $B_{00}(0)$. The B_{10} and B_{20} are the axisymmetric components and symmetric breaking terms with $n \neq 0$ are well limited within 1% even at the plasma edge at zero beta as shown in Fig. 3(a). As beta is increased, axisymmetric component B_{20} and B_{30} are enhanced with keeping symmetry breaking components relatively small.

Figure 4 shows the contours of B on the magnetic surface corresponding to $r/a = 0.5$ and the variation of B along the magnetic field line on that surface for (a) zero beta and (b) $\langle\beta\rangle = 1.15\%$ in collisional equilibrium. It is noted that the oblique line starting from (0,0) in top figures in Fig. 4 denotes the reference magnetic field line for one toroidal period. There is little deviation from axisymmetry at zero beta as expected from Fig. 3(a) and the enhancement of the axisymmetric components at finite beta makes the flattening of the variation of B in wide θ_B region as can be seen in Fig. 4(b). It implies that the magnetic configuration becomes close to omnigenous [21] on the inside as beta is increased, and this fact suggests that the particle drifts have a tendency to coincide with the magnetic surfaces on the inside.

3 Magnetic Configuration Control With Plasma Boundary Control

The basic properties of the reference QAS configuration are described in Section 2. The QAS properties are maintained even in the finite beta plasmas; however, the magnetic axis shift is rather large especially in collisional equilibrium. Therefore, the reduction of the magnetic axis shift or the Pfirsch-Schlüter current is important to obtain higher $\langle\beta\rangle_{eq}$ for wide operational regime. The Pfirsch-Schlüter current depends on the magnetic field topology for quasi-axisymmetry as [19]

$$\left|\frac{\boldsymbol{J}_{PS}}{B}\right| \propto \frac{1}{\iota}\left(\frac{1}{B^2} - \frac{1}{\langle B^2\rangle}\right). \tag{4}$$

Therefore, in order to reduce the Pfirsch-Schlüter current in finite beta quasi-axisymmetric equilibria, it is crucial to obtain higher ι and/or to reduce the modulation of B on the magnetic surface. In this section, these approaches are explained based on the plasma boundary control.

The plasma boundary can be Fourier decomposed in the cylindrical coordinates (R, ϕ, Z) as

$$\begin{aligned} R(s,\theta,\zeta) &= \sum_{mn} R_{mn}(s)\cos(m\theta - n\zeta), \\ Z(s,\theta,\zeta) &= \sum_{mn} Z_{mn}(s)\sin(m\theta - n\zeta), \end{aligned}$$

where s is the label of the magnetic surface and θ (ζ) is the poloidal (toroidal) angle in the VMEC coordinates [15].

In the following, the effects of the important boundary harmonics on the magnetic configuration are described. We chose the exact axisymmetric configuration described by $R_{00} = 2.0$ m, $R_{10} = 0.4$ m, $Z_{00} = 0.0$ m and $Z_{10} = 0.6$ m as the basic configuration. This configuration corresponds to the tokamak configuration without plasma current, and therefore, the rotational transform is exactly zero. The vacuum magnetic well depth is about 0.7%.

3.1 vertical elongation: Z_{10}

Increasing the vertical elongation is effective to decrease the plasma aspect ratio without increasing the toroidicity in the magnetic field spectra as listed in Table I. The $B_{10}/(a/R)$ is the ratio of the toroidicity in the magnetic field to the geometrical inverse aspect ratio. When the vertical elongation is increased, this ratio decreases, which implies that the toroidicity in magnetic field is effectively reduced.

The vertical elongation is also effective to decrease the modulation of B on the magnetic surface. Figure 5 shows the mod$-B$ contours and the outermost magnetic surface for Z_{10}/R_{10} = (a) 1.5 and (b) 2.0. It is noted that the magnetic surfaces have a tendency to coincide with mod$-B$ contours for larger Z_{10}/R_{10} case as shown in Fig. 5.

3.2 helical modulation: R_{11}, Z_{11}

When we put the helical harmonic R_{11} with $R_{11}/R_{10} = -0.5$ on the basic configuration. the magnetic surface cross section changes as shown in Fig. 6.1(a). The rotational transform increases up to $\iota \sim 0.1$ with enhancing the vacuum magnetic well up to about 1.3%. It can be seen in Fig. 6.2(a) that the bumpy or mirror harmonic with B_{01} is significantly enhanced with the opposite sign to B_{10} due to the flux conserving for the changes of the magnetic surface cross section.

As for Z_{11} with $Z_{11}/R_{10} = 0.5$, $\iota \sim 0.05$ and the vacuum magnetic well is significantly enhanced up to 6.9%. The bumpy harmonic B_{01} is substantially large with the same sign as that of B_{10} as shown in Fig. 6.2(b).

Therefore, one can expect that the fine combination of R_{11} and Z_{11} control allows to obtain the QAS configuration with higher rotational transform.

3.3 triangularity : Z_{21}

The harmonic Z_{21} can modify the triangularity ($m = 3$ component) due to the combination with R_{10} and Z_{10}. Since adding Z_{21} on the basic configuration causes little change in the magnetic properties, we increase the ratio of Z_{21}/R_{10} on the reference QAS configuration described in Section 2. Figure 7 shows the magnetic surface cross section with twice larger Z_{21}/R_{10} with keeping all other R_{mn}s and Z_{mn}s the same as those in reference QAS configuration. It can be seen that the cross section becomes more tear-drop like shape on $\phi = (1/4)(2\pi/M)$ and more triangular on $\phi = (1/2)(2\pi/M)$ compared to Fig. 1. The vacuum magnetic well is enhanced from 0.6% in reference QAS configuration to 4.1%. Therefore, it can be said that Z_{21} is effective to control the magnetic well depth.

One more important matter regarding to the magnetic field spectra is that B_{mn} depends on average radius generally as [22]

$$B_{mn} \propto (r/a)^m \,, \tag{5}$$

as shown in Fig. 8. It can be seen that B_{mn}s with low m have a larger amplitude than B_{mn}s with higher m around $r/a \sim 0.5$ where plasma density is relatively higher compared to the plasma edge region. Therefore, B_{mn}s with low m should be converted to B_{mn}s with higher m to realize the quasi-axisymmetric property around $r/a \sim 0.5$ by controlling R_{mn}s and Z_{mn}s with higher m number. One example is the control of R_{20}.

4 Examples of QAS Configurations Based on Plasma Boundary Control

In this section, we will describe two examples of QAS(-like) configurations obtained by the plasma boundary control explained in Section 3.

Figure 9 shows the magnetic surface cross section of the example 1 with higher rotational transform. It has been obtained by changing mainly R_{11}, Z_{11} and Z_{21} from the reference QAS configuration. The cross section on $\phi = 0$ is highly deformed by changing R_{11} and Z_{11} from Fig. 1 and the increase of Z_{21} makes the more tear-drop and triangular cross section on $\varphi = (1/4)(2\pi/M)$ and $\phi = (1/2)(2\pi/M)$, respectively. The vacuum rotational transform is $\iota(0)/\iota(a) = 0.42/0.47$ and this is about twice larger than reference QAS configuration. The vacuum magnetic well is also enhanced up to 3.4% due to the increase of Z_{21}. It is noted that the plasma aspect ratio is almost the same as reference QAS configuration. The magnetic axis shift in the collisional equilibrium is about 8.6% at $\langle\beta\rangle \sim 1\%$, which is significantly smaller than 37% in reference QAS configuration due to the higher rotational transform. This configuration is stable against ideal Mercier mode at least up to $\langle\beta\rangle \sim 1\%$.

The vacuum magnetic field spectra in the Boozer coordinates, the contours of B and the variation of B along the magnetic field line at $r/a = 0.5$ are shown in Fig. 10. The steep gradient of B_{00} corresponds to the deep vacuum magnetic well. From these figures, this configuration can be said to be close to QAS configuration, although there is a little deviation from axisymmetric variation of B due to the non-axisymmetric components as shown in Fig. 10(c).

In example 1, a fairly narrow cross section appears around $\phi = 0$ and this seems to be unfavorable for experiments. Therefore, we increased R_{10} to increase the width of the plasma cross section, resulting in the increase of the plasma minor radius or in the decrease of the plasma aspect ratio. In this case, the B_{10} increases and it becomes easier to cover or mask the non-axisymmetric contributions and to realize QAS configurations. This consideration has led to the example 2. We have reduced the modulation of B on the magnetic surface by vertically elongation Z_{10}, and R_{20} is controlled to convert B_{mn}s with $m = 1$ to B_{mn}s with higher m number.

The vacuum magnetic surface cross sections of the example 2 are shown in Fig. 11.

The strong bean shaped cross section arises from the increase of R_{20}. It should be noted that the plasma aspect ratio of this configuration is about 2.7 because of the large R_{10} and Z_{10}. The vacuum rotational transform $\iota(0)/\iota(a)$ is 0.25/0.29 with almost the same vacuum magnetic well as reference QAS configuration.

Figure 12.1 shows magnetic surface cross sections of example 2 at (a) $\langle\beta\rangle = 1.22\%$ for collisional equilibrium and (b) $\langle\beta\rangle = 1.26\%$ for collisionless equilibrium. The rotational transform and magnetic well depth for both equilibria are shown in Fig. 12.2. The calculated total bootstrap current is about 250 kA for collisionless equilibrium with the electron and ion density and temperature profiles, eqs. (2). The behavior of the rotational transform and well depth as beta is increased is almost the same as that in reference QAS configuration. The magnetic axis shift Δ/a is about 23% and 15% in the collisional and collisionless equilibrium, respectively, which are smaller to some extent than those in the reference QAS configuration. The ideal Mercier modes are evaluated to be stable in both equilibria except for the narrow edge region in collisionless equilibrium where the magnetic shear is rather weak as shown in Fig. 12.2(b).

The vacuum magnetic field spectra in Boozer coordinates, the contours of B and the variation of B along the magnetic field line on $r/a = 0.5$ are shown in Fig. 13. For reference, the plasma minor radius of the reference QAS configuration is shown by the arrow in Fig. 13(a). It is noted that $r/a = 0.5$ corresponds to the aspect ratio of about 5.4 in this configuration. There is very little deviation from axisymmetric variation of B as shown in Fig. 13(c) due to the large toroidicity B_{10} in magnetic field spectra and relatively small non-axisymmetric components. The non-axisymmetric components such as B_{21} and B_{22} have larger amplitude near the plasma edge due to the large plasma minor radius or small plasma aspect ratio. These components can be converted to B_{mn}s with higher m number; however, this configuration is not so far from the QAS configuration by considering that the outermost magnetic surface of reference QAS configuration corresponds to $r/a \sim 0.64$ in this configuration.

5 Summary

In order to improve the reflected particle confinement in stellarators, we have considered the quasi-axisymmetric stellarator (QAS) configurations with field period of $M = 2$. A reference QAS configuration has been obtained by optimization of the shape of the confinement region. The plasma aspect ratio of the reference QAS configuration is about 4.2 and $\iota(0)/\iota(a) = 0.23/0.28$ at zero beta. We have considered a wide operational regime such as (1) collisional equilibrium (high density, low temperature) without net plasma current and (2) collisionless equilibrium (low density, high temperature) with self-consistently calculated bootstrap current. The bootstrap current has an important role to increase the rotational transform in a wide plasma region, resulting in a reduction of the magnetic axis shift for obtaining higher $\langle\beta\rangle_{eq}$. Therefore, the bootstrap current is crucial in considering the optimization of QAS configurations.

However, the magnetic axis shift is significantly large in collisional equilibrium without net plasma current, and this implies that $\langle\beta\rangle_{eq}$ is rather low in this equilibrium. Therefore, we have considered the plasma boundary control for suppressing the Pfirsch-Schlüter current, that is, obtaining higher rotational transform and/or reducing the modulation of the magnetic field strength B on the magnetic surface. The effects of the important boundary harmonics are summarized as follows;

- vertically elongation: Z_{10} — reduction of plasma aspect ratio without increasing $|B_{10}|$ and reduction of modulation of B on magnetic surfaces,
- helical modulation: R_{11}, Z_{11} — increase of $\iota\!\!$- with significant enhancement of bumpy component B_{01},
- triangularity: Z_{21} — deepening of the vacuum magnetic well.

Since B_{mn} generally depends on r/a as $B_{mn} \propto (r/a)^m$, it is also important to convert B_{mn}s with lower m to B_{mn}s with higher m to realize the quasi-axisymmetry for a wide plasma core region.

Starting from the reference QAS configuration, we have obtained two QAS(-like) configurations. The example 1 has higher rotational transform (about twice larger than reference QAS configuration) with the plasma aspect ratio $A_p \sim 4.5$. The magnetic axis shift is significantly reduced even in the collisional equilibrium (1/4 of that in reference QAS configuration) based on changing R_{11}, Z_{11} for higher rotational transform, and Z_{21} for deeper vacuum magnetic well. As for the example 2, A_p decreases to about 2.7 due to the increase of R_{10} and Z_{10} for the reduction of the modulation of B on the magnetic surface. The B_{mn}s with $m = 1$ are well converted to B_{mn}s with higher m by R_{20} control. In this configuration, the magnetic axis shift reduces to about 2/3 of that in reference QAS configuration in the collisional equilibrium.

It is expected that QAS configuration can be obtained with $A_p \sim 3$ and much less magnetic axis shift compared to mentioned three QAS configurations by combining the plasma boundary control used to obtain example 1 and 2.

Finally, some future works are mentioned briefly.

We have examined MHD equilibria only up to $\langle\beta\rangle \sim 1\%$ and only ideal Mercier modes are considered as the first insight to MHD stability for comparison of several QAS configurations. Therefore, we should investigate $\langle\beta\rangle_{eq}$ and $\langle\beta\rangle_{st}$ in detail by considering also the resistive Mercier modes and ballooning modes.

We have used only the fixed boundary version of VMEC to obtain MHD equilibria; however, the plasma currents such as bootstrap current may change the plasma boundary. Therefore, we should also investigate free boundary equilibria. Moreover, the existence of the nested magnetic surfaces are assumed *a priori* in VMEC. The rotational transform has a weak shear in these $M = 2$ QAS configurations, and therefore, the behavior of magnetic islands should be examined. We will apply the HINT code [23] for this problem and clarify the effects of magnetic islands on MHD equilibrium and stability.

The experimental realization of QAS configurations, that is the external coil geometry, also should be considered by NESCOIL code, which also relates closely to the free boundary equilibria.

Acknowledgements

One of the authors (MY) gratefully acknowledges useful discussions with Prof. M. Wakatani and Dr. Y. Nakamura. Dr. P. Merkel is also appreciated for permission of use of the NESCOIL code.

References

[1] TODOROKI, J., et al., in Plasma Physics and Controlled Nuclear Fusion Research, 1988 (Proc. 12th Int. Conf. Nice), Vol.2, IAEA, Vienna (1989)637.

[2] IIYOSHI. A., et al., Fusion Technol. **17**(1990)169.

[3] GRIEGER, G., et al., Phys. Fluids **B4**(1992)2081.

[4] LOTZ, W., et al., Plasma Phys. Control. Fusion **34**(1992)1037.

[5] NÜHRENBERG, J., ZILLE, R., Phys. Lett **A129**(1988)113.

[6] ANDERSON, D. T., et al., HSX — A Helically Symmetric Toroidal Experiment — (edited by Torsatron/Stellarator Laboratory, Univ. of Wisconsin-Madison) (1993).

[7] HIRSHMAN, S. P., LEE, D. K., Comput. Phys. Commun. **39**(1986)161.

[8] NÜHRENBERG, J., ZILLE, R., Phys. Lett. **A114**(1986)129.

[9] NÜHRENBERG, J., in Theory of Fusion Plasmas (Proc. Workshop Varenna, 1994) Editrice Compositori, Bologna (1994)3.

[10] MERKEL, P., Nuclear Fusion **27**(1987)867.

[11] KIKUCHI, M., et al., Nucl. Fusion **30**(1990)343.

[12] TREFFERT, J. D., et al.. Phys. Rev. Lett. **53**(1984)2409.

[13] KIKUCHI, M., AZUMI, M., Plasma Phys. Control. Fusion **37**(1995)1215.

[14] GOLDSTON, R. J., Phys. Plasmas **3**(1996)1794.

[15] HIRSHMAN, S. P., et al., Comput. Phys. Commun. **43**(1986)143.

[16] OKAMURA, S., private communication (1996).

[17] WATANABE, K., NAKAJIMA, N., et al., Nuclear Fusion **35**(1995)335.

[18] GREENE, J. M., JOHNSON, J. L., Phys. Fluids **4**(1961)875.

[19] NAKAJIMA, N., OKAMOTO, M., J. Phys. Soc. Jpn. **61**(1992)833.

[20] BOOZER, A. H., Phys. Fluids **23**(1980)904.

[21] CATTO, P. J., HAZELTINE, R. D., Phys. Fluids **24**(1981)1663.

[22] MOROZOV, A. I., SOLOV'EV, L. S., Reviews of Plasma Physics, Vol.2, Consultants Bureau, New York (1966)p.1.

[23] HAYASHI. T., et al., Phys. Fluids **B4**(1992)1539.

Z_{10}/R_{10}	1.5	2.0
$B_{10}/(a/R)$	0.913	0.788

Table. I The ratio of the toroidicity in the magnetic field spectra B_{10} to the geometrical inverse aspect ratio for two different values of vertical elongation Z_{10}/R_{10}.

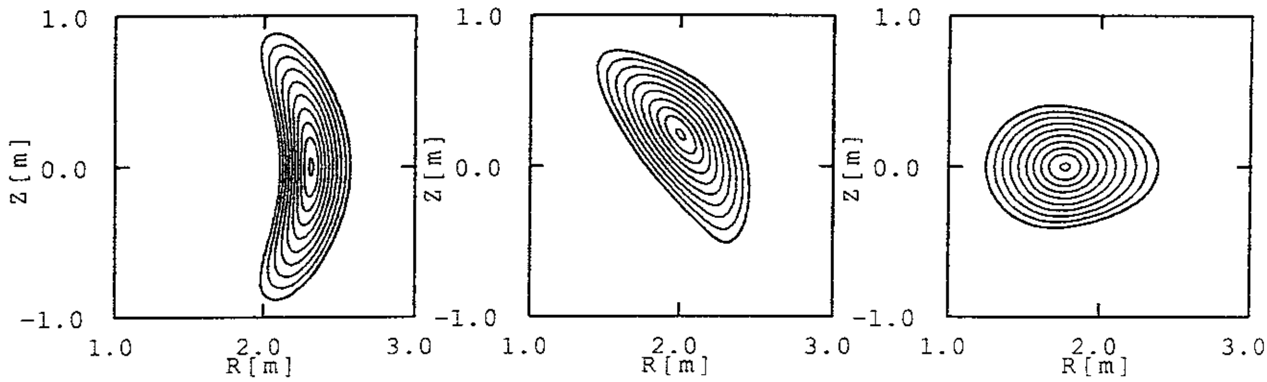

Fig. 1: Cross sections of vacuum magnetic surfaces of the reference QAS configuration on $\phi = 0$, $\phi = (1/4)(2\pi/M)$ and $\phi = (1/2)(2\pi/M)$, respectively.

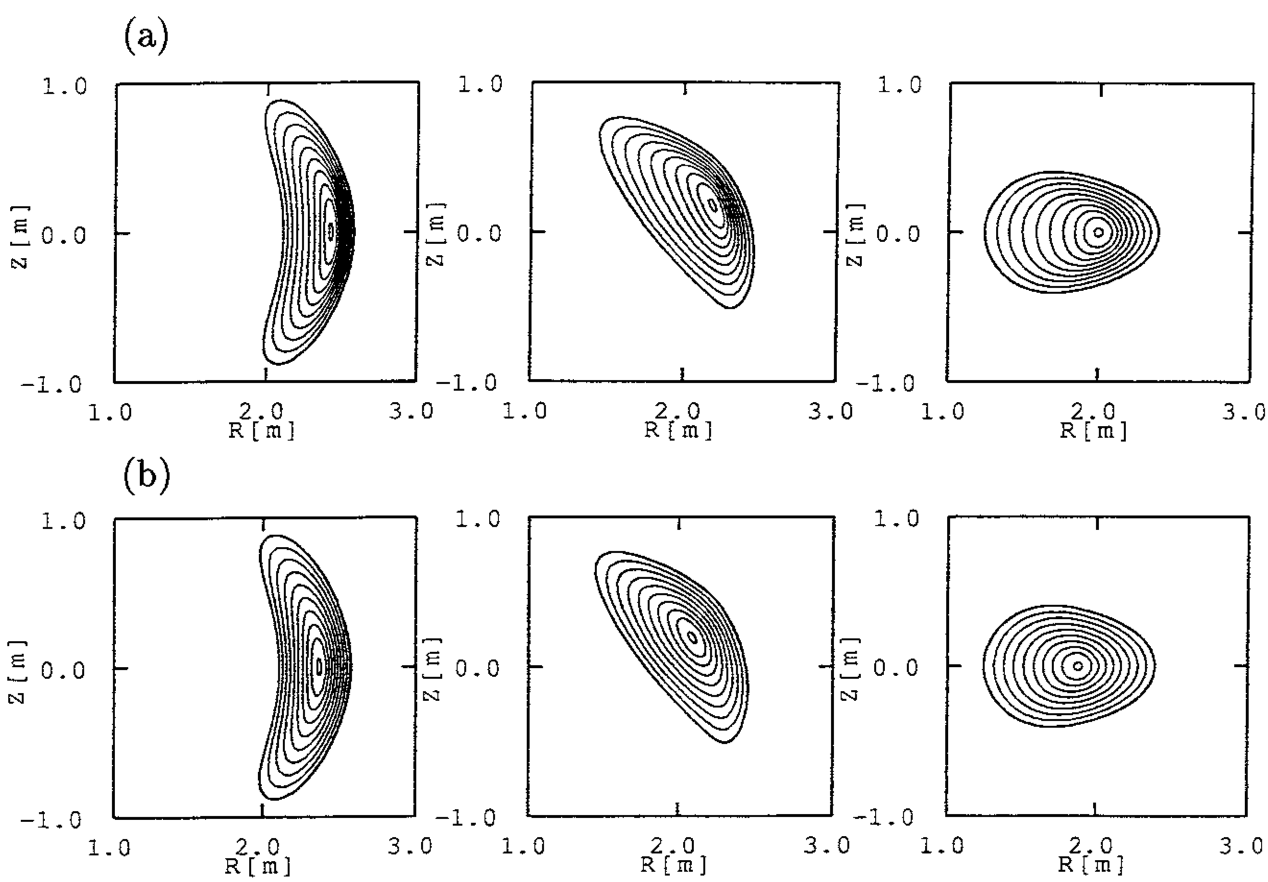

Fig. 2.1: Cross sections of magnetic surfaces of the reference QAS configuration at (a) $\langle\beta\rangle = 1.15\%$ for collisional equilibrium and (b) $\langle\beta\rangle = 1.18\%$ for collisionless equilibrium.

(a)

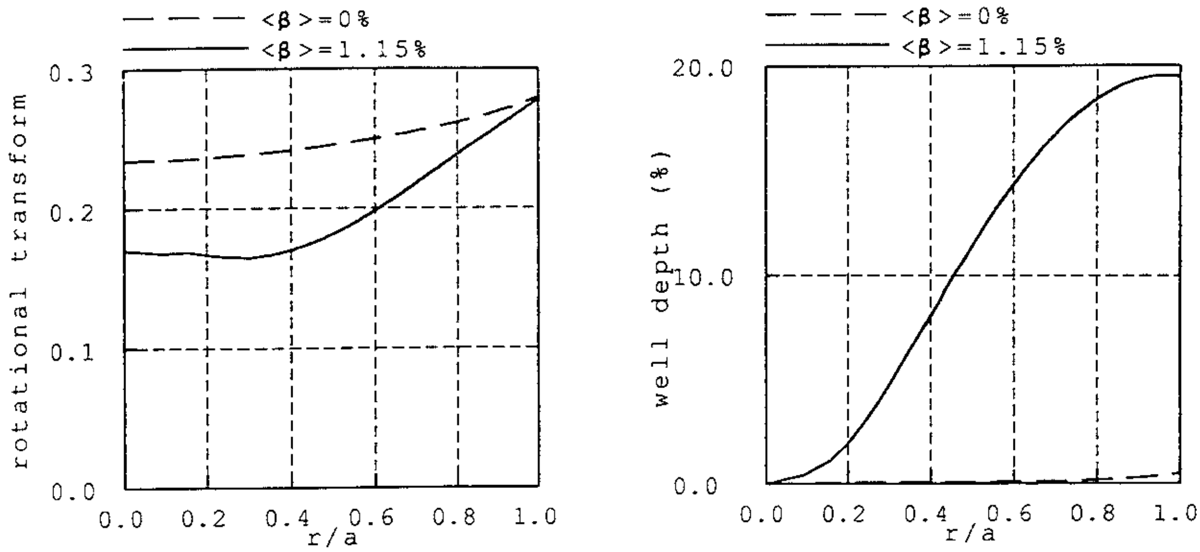

(b)

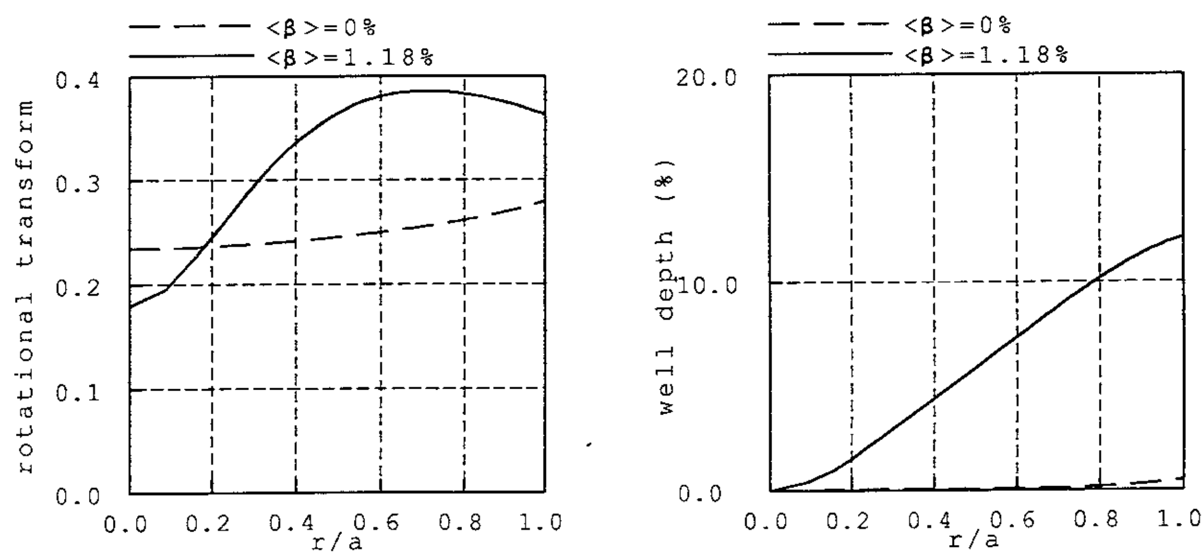

Fig. 2.2: Rotational transform (left) and magnetic well depth (right) of the reference QAS configuration at (a) $\langle\beta\rangle = 1.15\%$ for collisional equilibrium and (b) $\langle\beta\rangle = 1.18\%$ for collisionless equilibrium. The vacuum rotational transform and magnetic well depth are also shown.

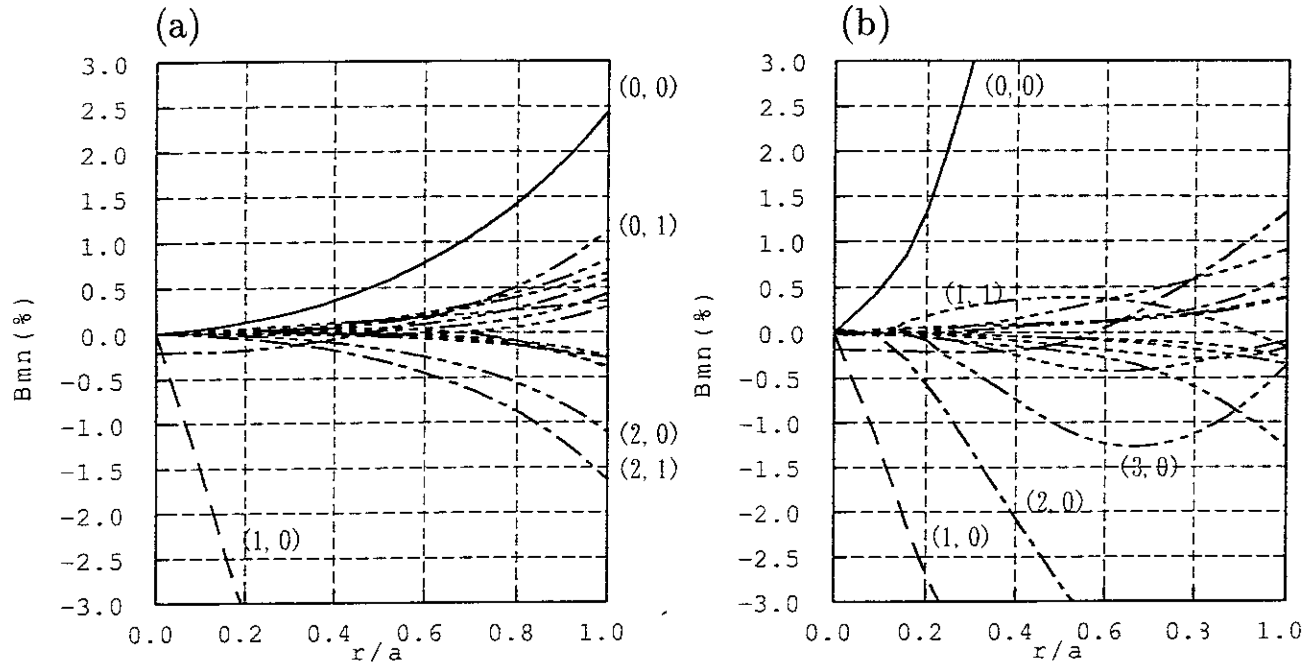

Fig. 3: Fourier spectra of the magnetic field strength in the Boozer coordinates for (a) zero beta and (b) collisional equilibrium at $\langle\beta\rangle = 1.15\%$.

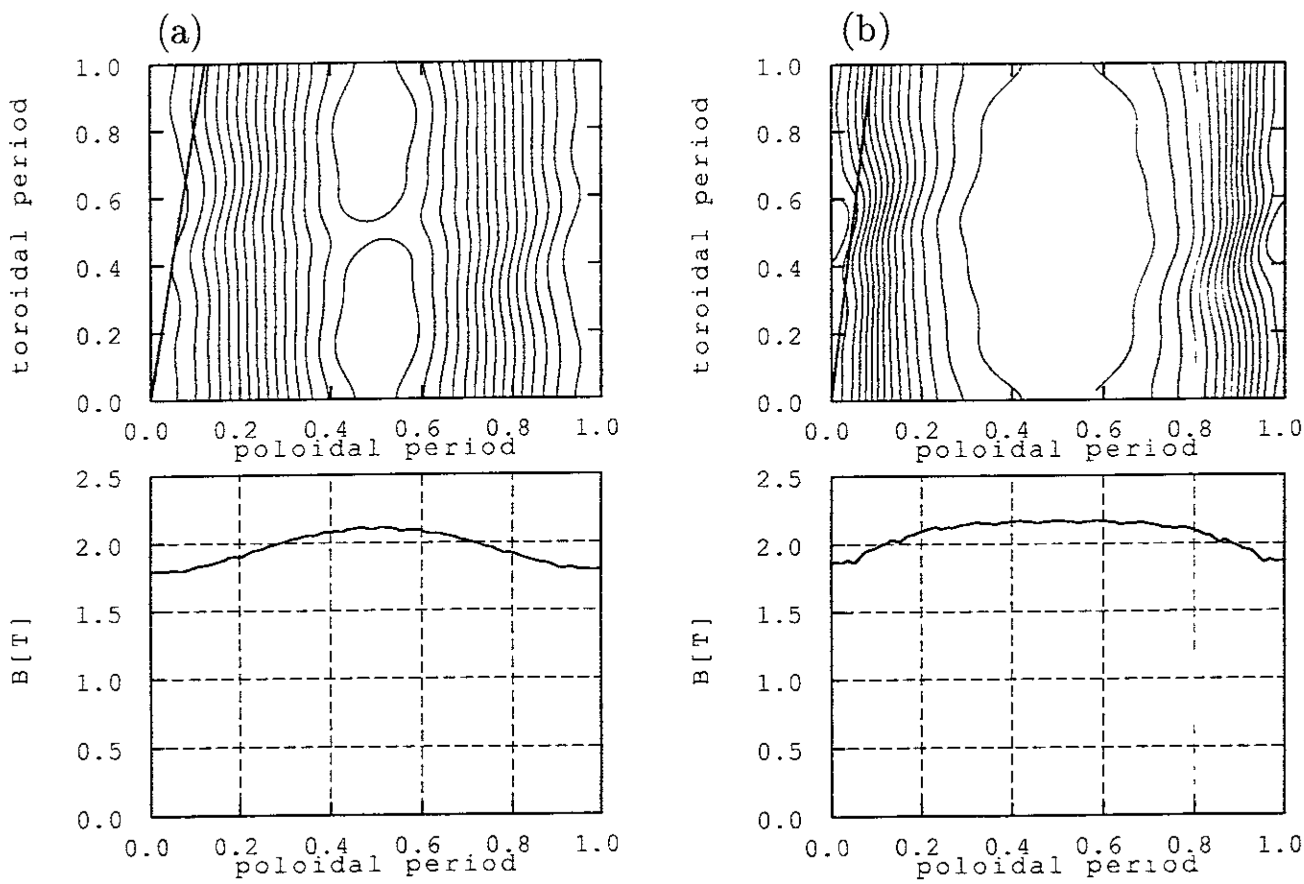

Fig. 4: Contours of the magnetic field strength on the (θ_B, ϕ_B) plane (top) and the magnetic field strength along the field line (bottom) both on $r/a = 0.5$ magnetic surface for (a) zero beta and (b) collisional equilibrium at $\langle\beta\rangle = 1.15\%$.

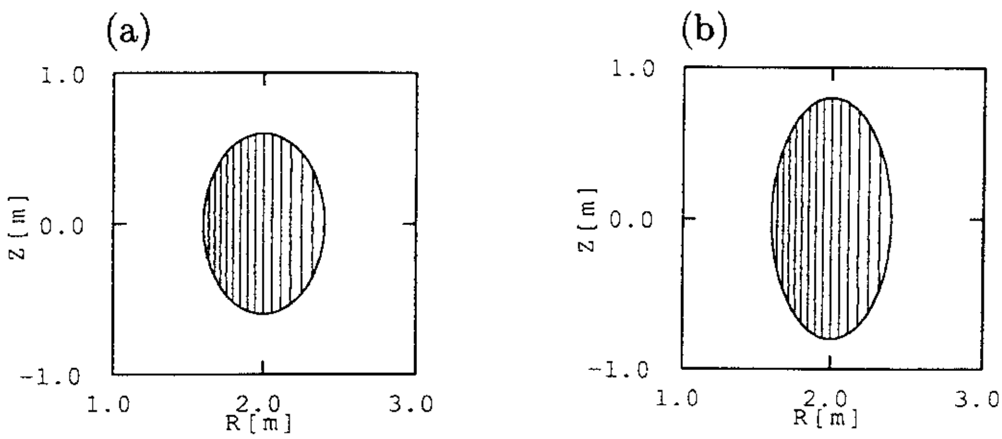

Fig. 5: The mod-B contours and the outermost magnetic surface are shown for (a) $Z_{10}/R_{10} = 1.5$ and (b) $Z_{10}/R_{10} = 2.0$.

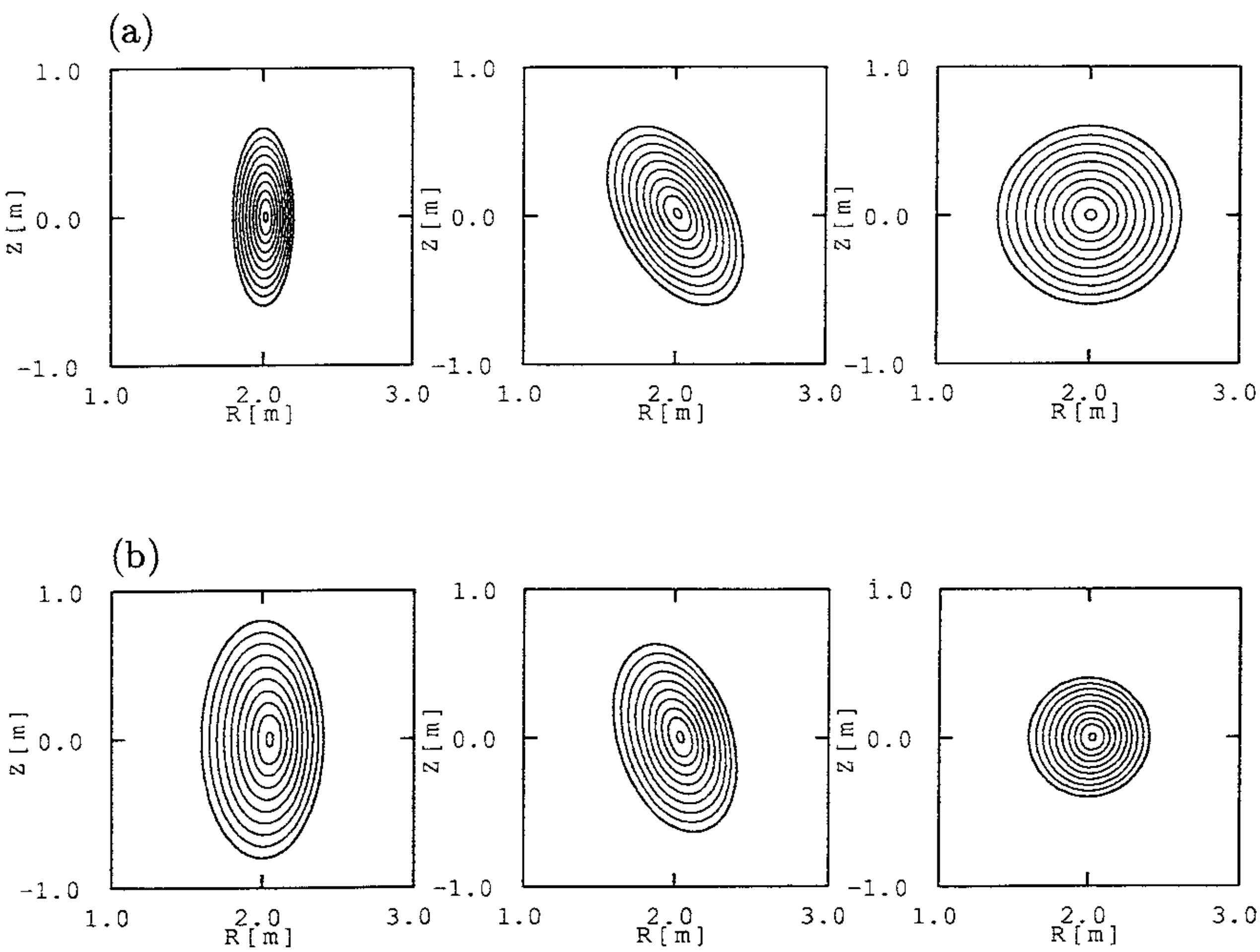

Fig. 6.1: Cross sections of vacuum magnetic surfaces when the helical modulation (a) $R_{11}/R_{10} = -0.5$ and (b) $Z_{11}/R_{10} = 0.5$ is added in the basic configuration.

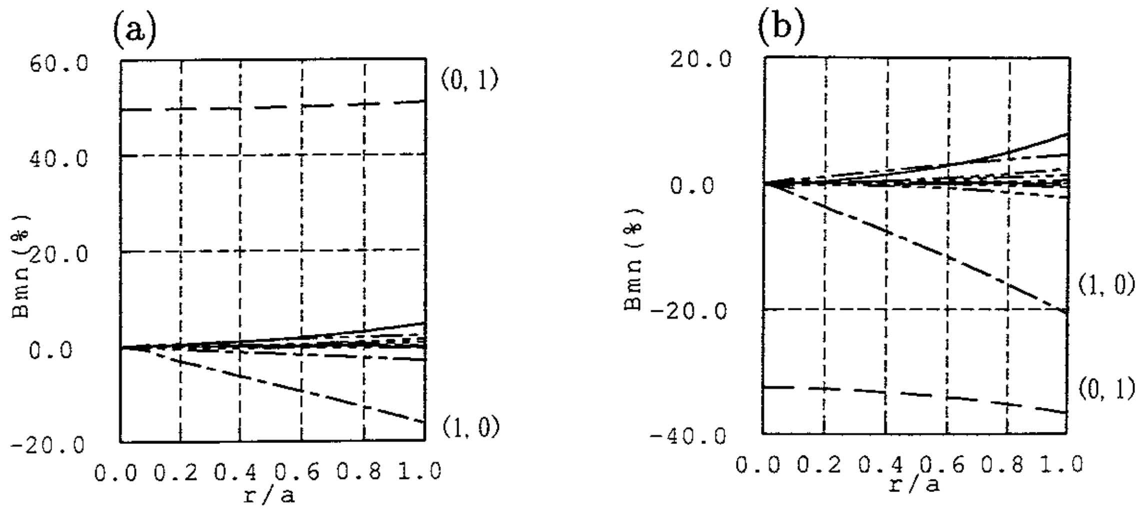

Fig. 6.2: Fourier spectra of the magnetic field strength in the Boozer coordinates for the magnetic configurations shown in Fig. 6.1(a) and (b), respectively.

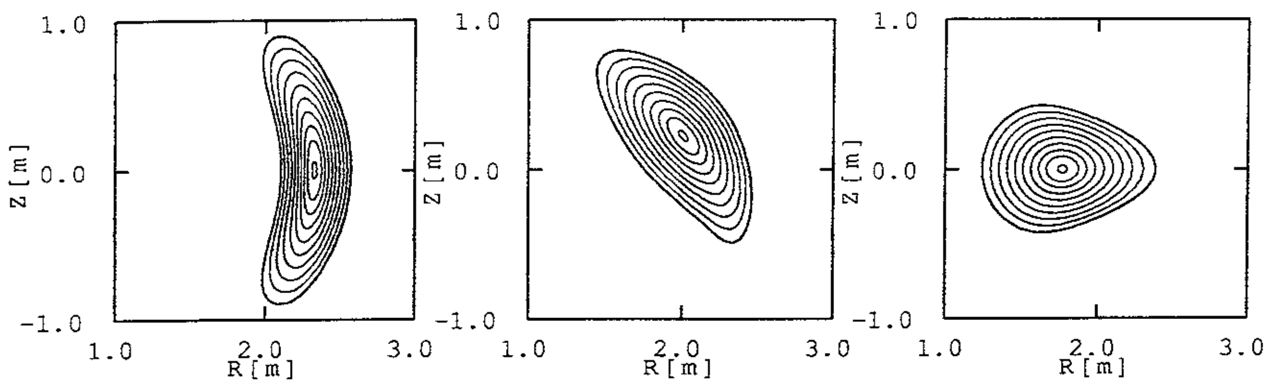

Fig. 7: Cross sections of vacuum magnetic surfaces when Z_{21}/R_{10} is doubled in the reference QAS configuration.

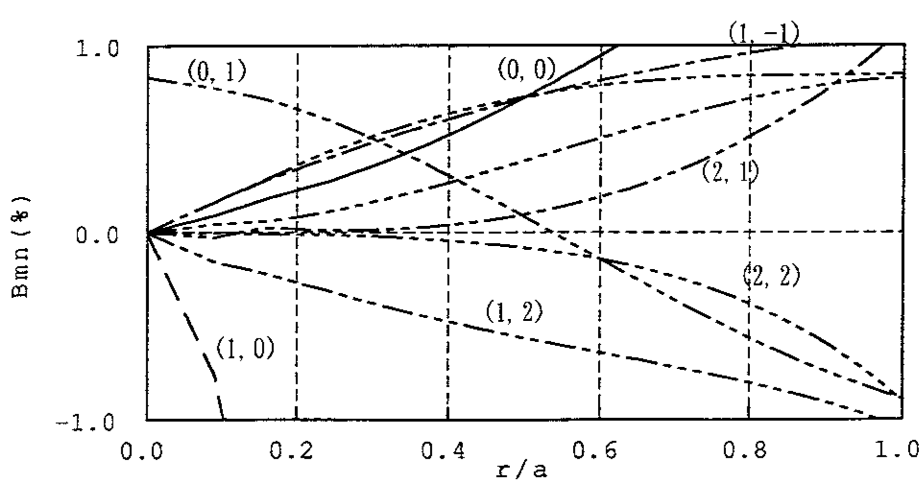

Fig. 8: The typical dependence of the magnetic spectra B_{mn}s on plasma radius.

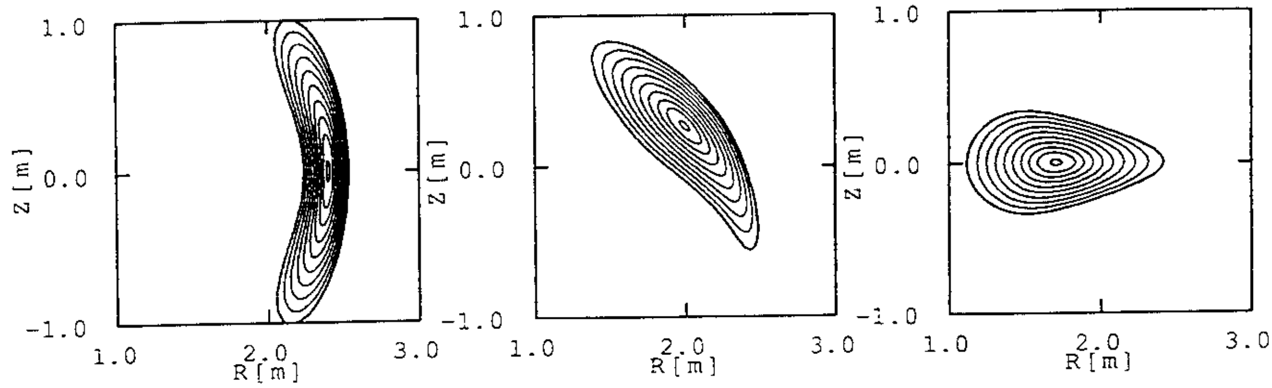

Fig. 9: Cross sections of the vacuum magnetic surfaces of QAS(-like) configuration (example 1).

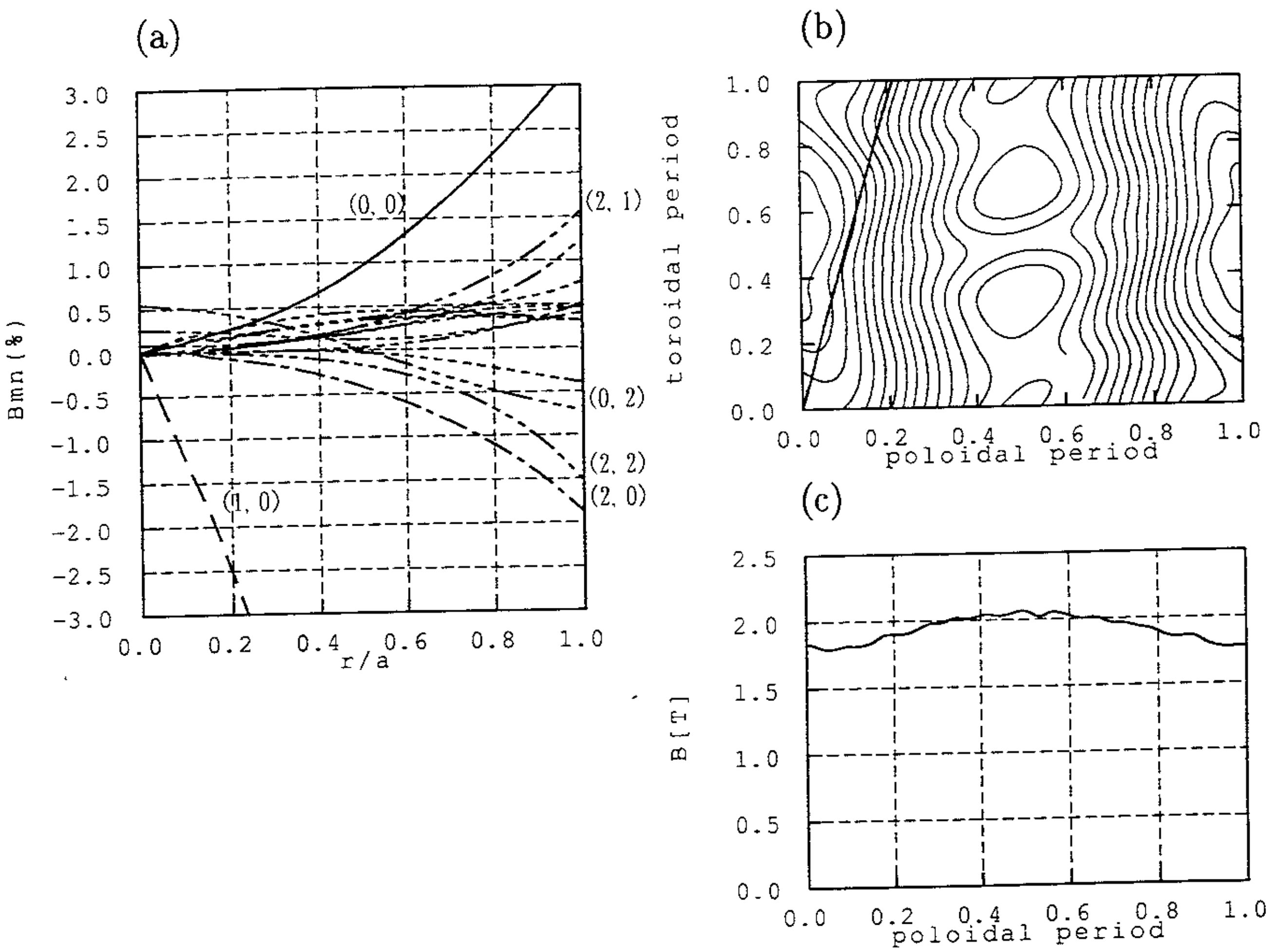

Fig. 10: (a) Fourier spectra of the magnetic field strength in the Boozer coordinates, (b) contours of the magnetic field strength on the (θ_B, ϕ_B) plane on $r/a = 0.5$ and (c) the magnetic field strength along the field line on $r/a = 0.5$ for QAS(-like) configuration (example 1) at zero beta.

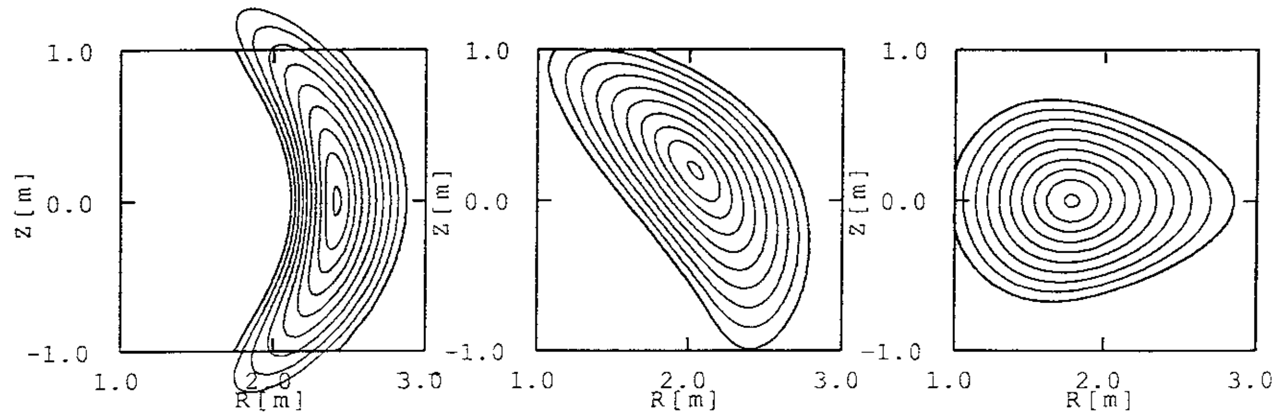

Fig. 11: Cross sections of the vacuum magnetic surfaces of QAS(-like) configuration (example 2).

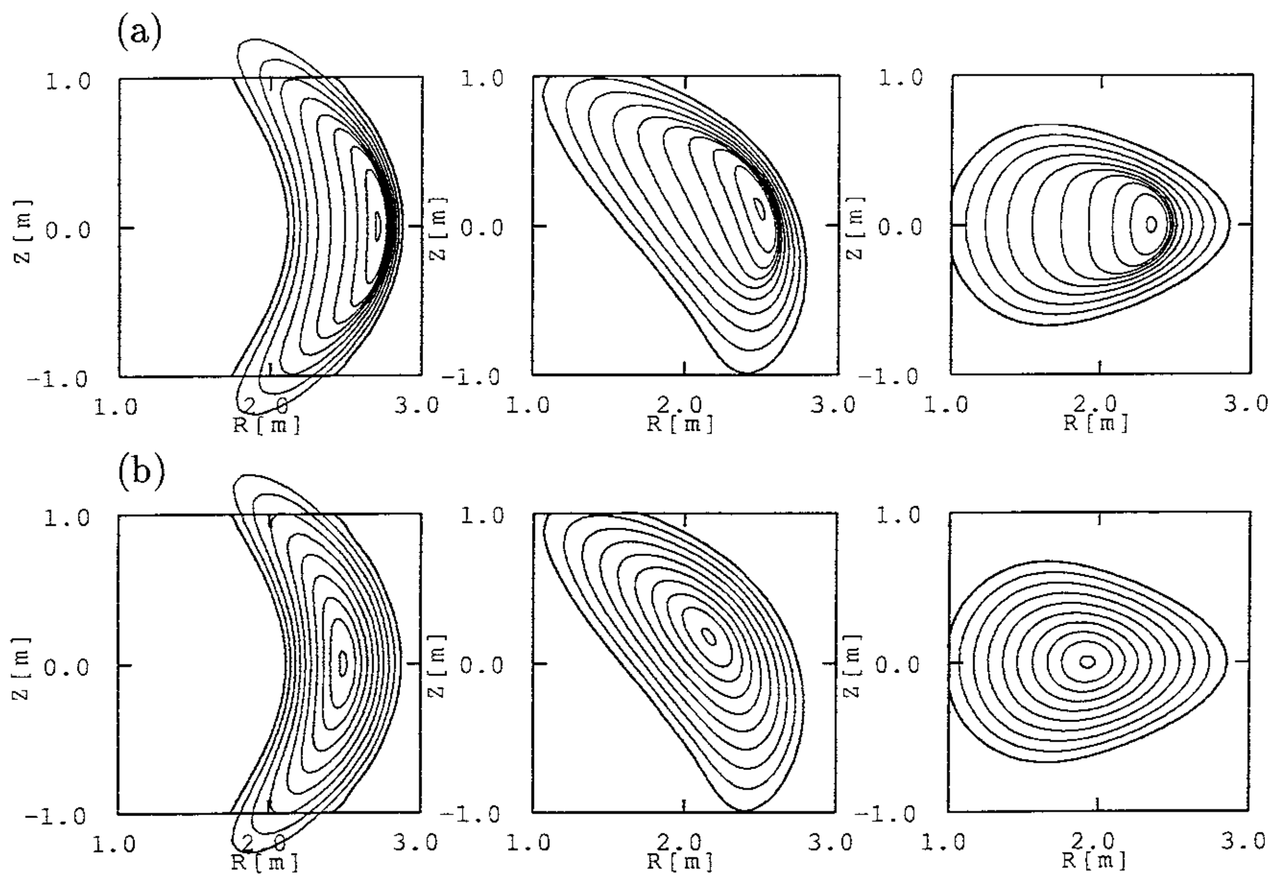

Fig. 12.1: Cross sections of magnetic surfaces of the configuration (example 2) at (a) $\langle\beta\rangle = 1.22\%$ for collisional equilibrium and (b) $\langle\beta\rangle = 1.26\%$ for collisionless equilibrium.

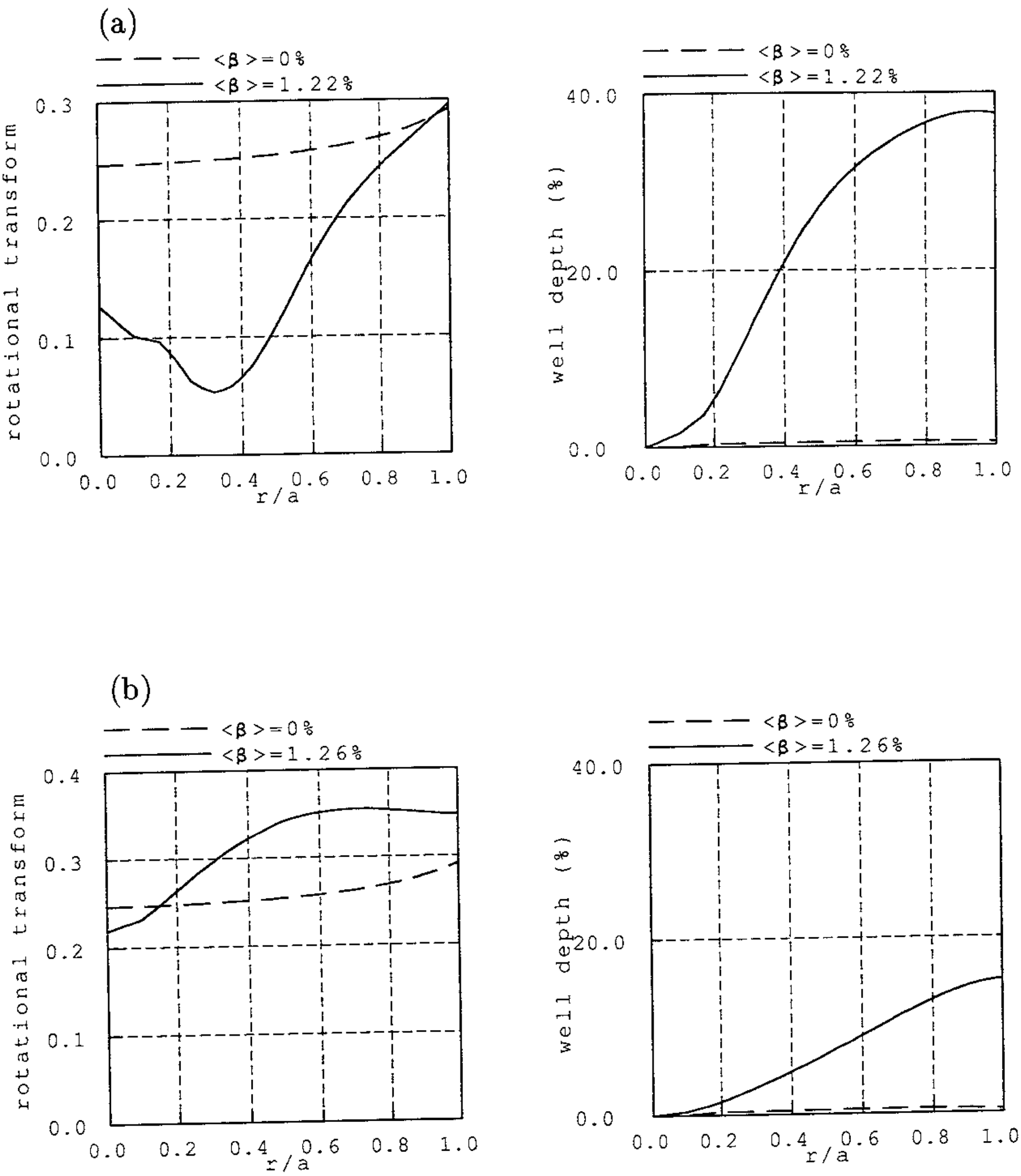

Fig. 12.2: Rotational transform (left) and magnetic well depth (right) of the configuration (example 2) at (a) $\langle\beta\rangle = 1.22\%$ for collisional equilibrium and (b) $\langle\beta\rangle = 1.26\%$ for collisionless equilibrium. The vacuum rotational transform and magnetic well depth are also shown.

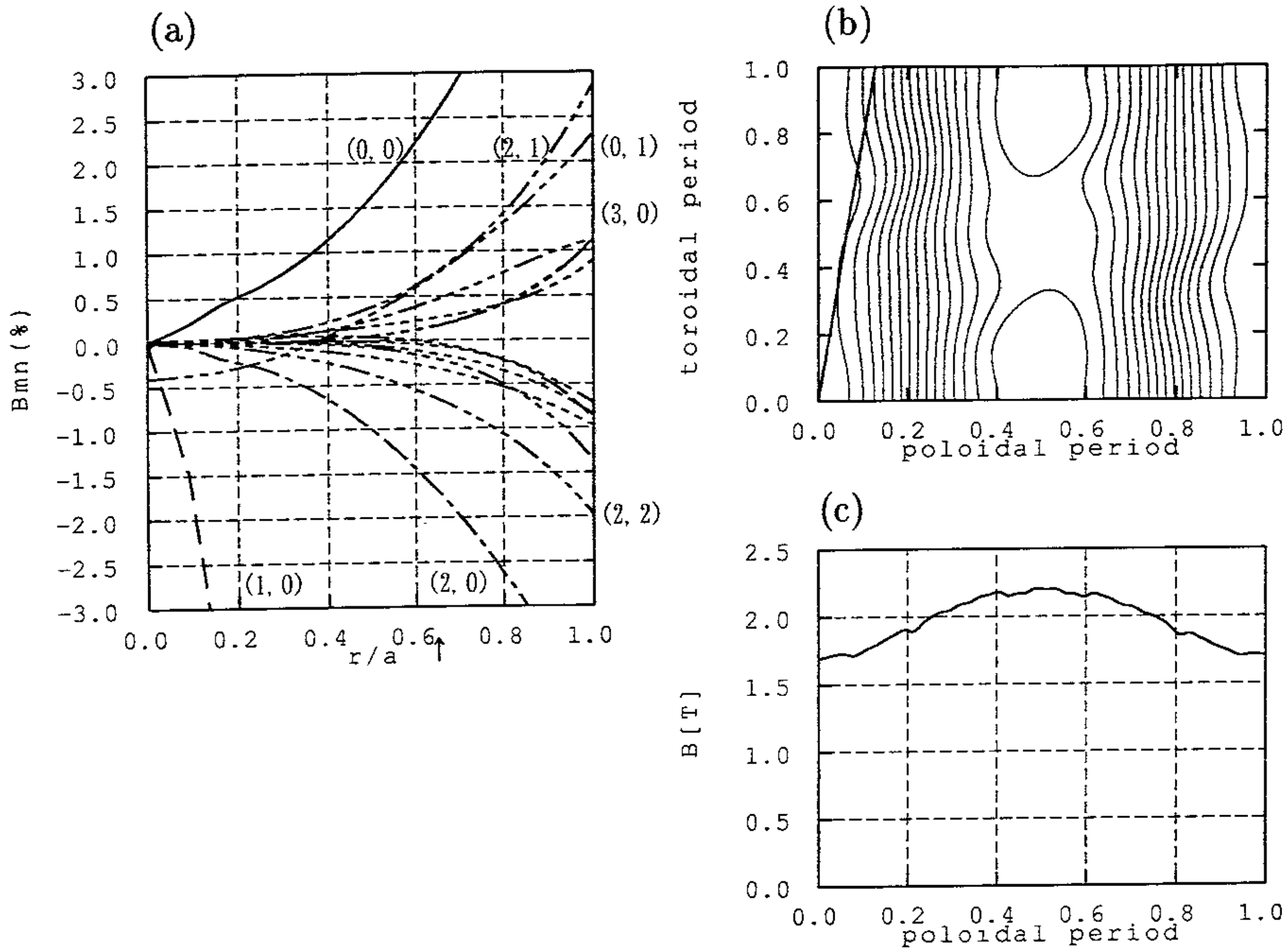

Fig. 13: (a) Fourier spectra of the magnetic field strength in the Boozer coordinates, (b) contours of the magnetic field strength on the (θ_B, ϕ_B) plane on $r/a = 0.5$ and (c) the magnetic field strength along the field line on $r/a = 0.5$ for QAS(-like) configuration (example 2) at zero beta.

Recent Issues of NIFS Series

NIFS-432 T.-H. Watanabe, T. Sato and T. Hayashi,
Magnetohydrodynamic Simulation on Co- and Counter-helicity Merging of Spheromaks and Driven Magnetic Reconnection; Aug. 1996

NIFS-433 R. Horiuchi and T. Sato,
Particle Simulation Study of Collisionless Driven Reconnection in a Sheared Magnetic Field; Aug. 1996

NIFS-434 Y. Suzuki, K. Kusano and K. Nishikawa,
Three-Dimensional Simulation Study of the Magnetohydrodynamic Relaxation Process in the Solar Corona. II.; Aug. 1996

NIFS-435 H. Sugama and W. Horton,
Transport Processes and Entropy Production in Toroidally Rotating Plasmas with Electrostatic Turbulence; Aug. 1996

NIFS-436 T. Kato, E. Rachlew-Källne, P. Hörling and K.-D Zastrow,
Observations and Modelling of Line Intensity Ratios of OV Multiplet Lines for 2s3s 3S1 - 2s3p 3Pj; Aug. 1996

NIFS-437 T. Morisaki, A. Komori, R. Akiyama, H. Idei, H. Iguchi, N. Inoue, Y. Kawai, S. Kubo, S. Masuzaki, K. Matsuoka, T. Minami, S. Morita, N. Noda, N. Ohyabu, S. Okamura, M. Osakabe, H. Suzuki, K. Tanaka, C. Takahashi, H. Yamada, I. Yamada and O. Motojima,
Experimental Study of Edge Plasma Structure in Various Discharges on Compact Helical System; Aug. 1996

NIFS-438 A. Komori, N. Ohyabu, S. Masuzaki, T. Morisaki, H. Suzuki, C. Takahashi, S. Sakakibara, K. Watanabe, T. Watanabe, T. Minami, S. Morita, K. Tanaka, S. Ohdachi, S. Kubo, N. Inoue, H. Yamada, K. Nishimura, S. Okamura, K. Matsuoka, O. Motojima, M. Fujiwara, A. Iiyoshi, C. C. Klepper, J.F. Lyon, A.C. England, D.E. Greenwood, D.K. Lee, D.R. Overbey, J.A. Rome, D.E. Schechter and C.T. Wilson,
Edge Plasma Control by a Local Island Divertor in the Compact Helical System; Sep. 1996 (IAEA-CN-64/C1-2)

NIFS-439 K. Ida, K. Kondo, K. Nagaski T. Hamada, H. Zushi, S. Hidekuma, F. Sano, T. Mizuuchi, H. Okada, S. Besshou, H. Funaba, Y. Kurimoto, K. Watanabe and T. Obiki,
Dynamics of Ion Temperature in Heliotron-E; Sep. 1996 (IAEA-CN-64/CP-5)

NIFS-440 S. Morita, H. Idei, H. Iguchi, S. Kubo, K. Matsuoka, T. Minami, S. Okamura, T. Ozaki, K. Tanaka, K. Toi, R. Akiyama, A. Ejiri, A. Fujisawa, M. Fujiwara, M. Goto, K. Ida, N. Inoue, A. Komori, R. Kumazawa, S. Masuzaki, T. Morisaki, S. Muto, K. Narihara, K. Nishimura, I. Nomura, S. Ohdachi, M.. Osakabe, A. Sagara, Y. Shirai, H. Suzuki, C. Takahashi, K. Tsumori, T. Watari, H. Yamada and I. Yamada, *A Study on Density Profile and Density Limit of NBI Plasmas in CHS*; Sep. 1996 (IAEA-CN-64/CP-3)

NIFS-441 O. Kaneko, Y. Takeiri, K. Tsumori, Y. Oka, M. Osakabe, R. Akiyama, T. Kawamoto, E. Asano and T. Kuroda,
Development of Negative-Ion-Based Neutral Beam Injector for the Large Helical Device; Sep. 1996 (IAEA-CN-64/GP-9)

NIFS-442 K. Toi, K.N. Sato, Y. Hamada, S. Ohdachi, H. Sakakita, A. Nishizawa, A. Ejiri, K. Narihara, H. Kuramoto, Y. Kawasumi, S. Kubo, T. Seki, K. Kitachi, J. Xu, K. Ida, K. Kawahata, I. Nomura, K. Adachi, R. Akiyama, A. Fujisawa, J. Fujita, N. Hiraki, S. Hidekuma, S. Hirokura, H. Idei, T. Ido, H. Iguchi, K. Iwasaki, M. Isobe, O. Kaneko. Y. Kano, M. Kojima, J. Koog, R. Kumazawa, T. Kuroda, J. Li, R. Liang, T. Minami, S. Morita, K. Ohkubo, Y. Oka, S. Okajima, M. Osakabe, Y. Sakawa, M. Sasao, K. Sato, T. Shimpo, T. Shoji, H. Sugai, T. Watari, I. Yamada and K. Yamauti,
Studies of Perturbative Plasma Transport, Ice Pellet Ablation and Sawtooth Phenomena in the JIPP T-IIU Tokamak; Sep. 1996 (IAEA-CN-64/A6-5)

NIFS-443 Y. Todo, T. Sato and The Complexity Simulation Group,
Vlasov-MHD and Particle-MHD Simulations of the Toroidal Alfvén Eigenmode; Sep. 1996 (IAEA-CN-64/D2-3)

NIFS-444 A. Fujisawa, S. Kubo, H. Iguchi, H. Idei, T. Minami, H. Sanuki, K. Itoh, S. Okamura, K. Matsuoka, K. Tanaka, S. Lee, M. Kojima, T.P. Crowley, Y. Hamada, M. Iwase, H. Nagasaki, H. Suzuki, N. Inoue, R. Akiyama, M. Osakabe, S. Morita, C. Takahashi, S. Muto, A. Ejiri, K. Ida, S. Nishimura, K. Narihara, I. Yamada, K. Toi, S. Ohdachi, T. Ozaki, A. Komori, K. Nishimura, S. Hidekuma, K. Ohkubo, D.A. Rasmussen, J.B. Wilgen, M. Murakami, T. Watari and M. Fujiwara,
An Experimental Study of Plasma Confinement and Heating Efficiency through the Potential Profile Measurements with a Heavy Ion Beam Probe in the Compact Helical System; Sep. 1996 (IAEA-CN-64/C1-5)

NIFS-445 O. Motojima, N. Yanagi, S. Imagawa, K. Takahata, S. Yamada, A. Iwamoto, H. Chikaraishi, S. Kitagawa, R. Maekawa, S. Masuzaki, T. Mito, T. Morisaki, A. Nishimura, S. Sakakibara, S. Satoh, T. Satow, H. Tamura, S. Tanahashi, K. Watanabe, S. Yamaguchi, J. Yamamoto, M.Fujiwara and A. Iiyoshi,
Superconducting Magnet Design and Construction of LHD; Sep. 1996 (IAEA-CN-64/G2-4)

NIFS-446 S. Murakami, N. Nakajima, S. Okamura, M. Okamoto and U. Gasparino,
Orbit Effects of Energetic Particles on the Reachable β–Value and the Radial Electric Field in NBI and ECR Heated Heliotron Plasmas; Sep. 1996 (IAEA-CN-64/CP -6) Sep. 1996

NIFS-447 K. Yamazaki, A. Sagara, O. Motojima, M. Fujiwara, T. Amano, H. Chikaraishi, S. Imagawa, T. Muroga, N. Noda, N. Ohyabu, T. Satow, J.F. Wang, K.Y. Watanabe, J. Yamamoto . H. Yamanishi, A. Kohyama, H. Matsui, O. Mitarai, T. Noda, A.A. Shishkin, S. Tanaka and T. Terai
Design Assessment of Heliotron Reactor; Sep. 1996

(IAEA-CN-64/G1-5)

NIFS-448 M. Ozaki, T. Sato and the Complexity Simulation Group,
Interactions of Convecting Magnetic Loops and Arcades; Sep. 1996

NIFS-449 T. Aoki,
Interpolated Differential Operator (IDO) Scheme for Solving Partial Differential Equations; Sep. 1996

NIFS-450 D. Biskamp and T. Sato,
Partial Reconnection in the Sawtooth Collapse; Sep. 1996

NIFS-451 J. Li, X. Gong, L. Luo, F.X. Yin, N. Noda, B. Wan, W. Xu, X. Gao, F. Yin, J.G. Jiang, Z. Wu., J.Y. Zhao, M. Wu, S. Liu and Y. Han,
Effects of High Z Probe on Plasma Behavior in HT-6M Tokamak; Sep. 1996

NIFS-452 N. Nakajima, K. Ichiguchi, M. Okamoto and R.L. Dewar,
Ballooning Modes in Heliotrons/Torsatrons; Sep. 1996 (IAEA-CN-64/D3-6)

NIFS-453 A. Iiyoshi,
Overview of Helical Systems; Sep. 1996 (IAEA-CN-64/O1-7)

NIFS-454 S. Saito, Y. Nomura, K. Hirose and Y.H. Ichikawa,
Separatrix Reconnection and Periodic Orbit Annihilation in the Harper Map; Oct. 1996

NIFS-455 K. Ichiguchi, N. Nakajima and M. Okamoto,
Topics on MHD Equilibrium and Stability in Heliotron / Torsatron; Oct. 1996

NIFS-456 G. Kawahara, S. Kida, M. Tanaka and S. Yanase,
Wrap, Tilt and Stretch of Vorticity Lines around a Strong Straight Vortex Tube in a Simple Shear Flow; Oct. 1996

NIFS-457 K. Itoh, S.- I. Itoh. A. Fukuyama and M. Yagi,
Turbulent Transport and Structural Transition in Confined Plasmas; Oct. 1996

NIFS-458 A. Kageyama and T. Sato,
Generation Mechanism of a Dipole Field by a Magnetohydrodynamic Dynamo; Oct. 1996

NIFS-459 K. Araki, J. Mizushima and S. Yanase,
The Non-axisymmetric Instability of the Wide-Gap Spherical Couette Flow; Oct. 1996

NIFS-460 Y. Hamada, A. Fujisawa, H. Iguchi, A. Nishizawa and Y. Kawasumi,
A Tandem Parallel Plate Analyzer; Nov. 1996

NIFS-461 Y. Hamada, A. Nishizawa, Y. Kawasumi, A. Fujisawa, K. Narihara, K. Ida, A. Ejiri, S. Ohdachi, K. Kawahata, K. Toi, K. Sato, T. Seki, H. Iguchi, K. Adachi, S. Hidekuma, S.Hirokura, K. Iwasaki, T. Ido, M. Kojima, J. Koong, R. Kumazawa, H. Kuramoto, T. Minami, I. Nomura, H. Sakakita, M. Sasao, K.N. Sato, T. Tsuzuki, J. Xu, I. Yamada and T. Watari,
Density Fluctuation in JIPP T-IIU Tokamak Plasmas Measured by a Heavy Ion Beam Probe; Nov. 1996

NIFS-462 N. Katsuragawa, H. Hojo and A. Mase,
Simulation Study on Cross Polarization Scattering of Ultrashort-Pulse Electromagnetic Waves; Nov. 1996

NIFS-463 V. Voitsenya, V. Konovalov, O. Motojima, K. Narihara, M. Becker and B. Schunke,
Evaluations of Different Metals for Manufacturing Mirrors of Thomson Scattering System for the LHD Divertor Plasma; Nov. 1996

NIFS-464 M. Pereyaslavets, M. Sato, T. Shimozuma, Y. Takita, H. Idei, S. Kubo, K. Ohkubo and K. Hayashi,
Development and Simulation of RF Components for High Power Millimeter Wave Gyrotrons; Nov. 1997

NIFS-465 V.S. Voitsenya, S. Masuzaki, O. Motojima, N. Noda and N. Ohyabu,
On the Use of CX Atom Analyzer for Study Characteristics of Ion Component in a LHD Divertor Plasma; Dec. 1996

NIFS-466 H. Miura and S. Kida,
Identification of Tubular Vortices in Complex Flows; Dec. 1996

NIFS-467 Y. Takeiri, Y. Oka, M. Osakabe, K. Tsumori, O. Kaneko, T. Takanashi, E. Asano, T. Kawamoto, R. Akiyama and T. Kuroda,
Suppression of Accelerated Electrons in a High-current Large Negative Ion Source; Dec. 1996

NIFS-468 A. Sagara. Y. Hasegawa, K. Tsuzuki, N. Inoue, H. Suzuki, T. Morisaki, N. Noda, O. Motojima, S. Okamura, K. Matsuoka, R. Akiyama, K. Ida, H. Idei, K. Iwasaki, S. Kubo, T. Minami, S. Morita, K. Narihara, T. Ozaki, K. Sato, C. Takahashi, K. Tanaka, K. Toi and I. Yamada,
Real Time Boronization Experiments in CHS and Scaling for LHD; Dec. 1996

NIFS-469 V.L. Vdovin, T.Watari and A. Fukuyama,
3D Maxwell-Vlasov Boundary Value Problem Solution in Stellarator Geometry in Ion Cyclotron Frequency Range (final report); Dec. 1996

NIFS-470 N. Nakajima, M. Yokoyama, M. Okamoto and J. Nührenberg,
Optimization of M=2 Stellarator; Dec. 1996